Viscous fingering in packed chromatographic columns: Non-linear dynamics

G. Rousseaux [a,c], M. Martin [b], A. De Wit [c,*]

[a] Université de Nice Sophia Antipolis, Laboratoire J.-A. Dieudonné UMR 6621 CNRS-UNS, Parc Valrose, 06108 Nice Cedex 02, France
[b] Ecole Supérieure de Physique et de Chimie Industrielles, Laboratoire de Physique et Mécanique des Milieux Hétérogènes (PMMH, UMR 7636 CNRS, ESPCI ParisTech, Université Pierre et Marie Curie, Université Paris-Diderot), 10 rue Vauquelin, 75231 Paris Cedex 05, France
[c] Nonlinear Physical Chemistry Unit, Service de Chimie Physique et Biologie Théorique, Faculté des Sciences, Université Libre de Bruxelles (ULB), CP231, 1050 Brussels, Belgium

ARTICLE INFO

ABSTRACT

Viscous fingering (VF) is a hydrodynamic instability that occurs in a chromatographic column when a less viscous fluid displaces another more viscous one. This instability is detrimental to separation techniques as it leads to distorted peaks and peak broadening. Nonlinear interactions between developing fingers lead to complex dynamics investigated in the present study by means of numerical simulations based on a simple model for miscible VF of finite samples. We review the properties of nonlinear VF and discuss the quantitative measures that can be applied both on such numerical as well as on experimental data to gain insight into the influence of the parameters of the problem on the nonlinear properties of the fingers and on the broadening of output peaks.

© 2011 Elsevier B.V. All rights reserved.

1. Introduction

In the most common form of liquid chromatography, the eluent separates the different chemical species of the sample by displacing them selectively through a porous medium already filled with that eluent. As the sample usually has a viscosity different from that of the eluent, its displacement inside the porous column can be influenced by a hydrodynamic viscous fingering (VF) instability. VF occurs in a porous medium as soon as a fluid of given viscosity η_1 displaces another more viscous one of viscosity $\eta_2 > \eta_1$. The interface between the two fluids does not remain flat anymore but is deformed into "fingers" of one fluid invading the other one. Because this fingering is increasing the mixing between the two fluids, it is particularly detrimental to oil recovery where VF occurs when water is displacing oil in underground reservoirs. This explains why the VF instability has been much studied in the petroleum engineering literature (see [1] for a review). More fundamental approaches [1–3] have also been developed in the physics literature especially following the experimental work of Saffman and Taylor [4] and Wooding [5] who have studied experimentally VF between two immiscible and miscible fluids respectively in a Hele-Shaw cell [6]. Such a cell consists in two parallel glass or plastic plates separated by a thin gap in which the dynamics of fluids is easy to visualize and to follow by a camera [7]. In such cells, the evolution equations for the flow velocity averaged across the gap thickness are analog to Darcy's law provided the gap thickness is thin enough compared

to the length and width of the plates. Since then, numerous theoretical and experimental studies have allowed to gain insight into the properties of VF of one single interface. Models vary depending whether the fluids are immiscible (in which case surface tension is a stabilizing factor favoring a flat interface) or miscible (where diffusion or dispersion is stabilizing as it favors a reduction in time of the initial viscosity jump across the interface and smoothes out transverse perturbations). In both cases, the source of the instability, its driving motor, is the amplitude of the viscosity ratio η_2/η_1 between the two fluids. The larger this ratio, the more unstable the interface. As applications in chromatography are related to miscible VF rather than immiscible VF, we will in the sequel only further discuss miscible VF. Thanks to numerous works (see [1,3,7–18] and refs therein), the basic features of miscible VF of one interface are nowadays well understood. VF takes place as soon as the viscosity ratio η_2/η_1 is larger than 1. The system is more unstable at large injection speed (large Peclet number) and small transverse dispersion. At onset, the finger width (or, more precisely, their wavelength since hydrodynamic instabilities are most generally described as wave systems) and onset time of the VF pattern can be predicted by a linear stability analysis [8,9,19]. At later times, the fingers grow and interact in complex nonlinear dynamics which have been described experimentally and numerically in details [1,4,5,7,10–15].

In this context, understanding VF in chromatographic columns is of particular interest because this instability is detrimental to the separation performances [20–38]. Any improvement that would allow to reduce the influence of VF on peak tailing and band broadening would be of utmost importance. VF in chromatography has a peculiar feature with regard to VF of one single interface between two semi-infinite regions which is that the sample injected inside

* Corresponding author. Tel.: +32 2 6505774; fax: +32 2 6505767.
E-mail address: adewit@ulb.ac.be (A. De Wit).

the porous matrix is of finite width [31]. VF develops at the frontal interface where the sample pushes the eluent if the sample is less viscous than the carrying fluid [27–29,32,39,40]. On the contrary, VF is observed at the rear interface if the sample is more viscous than the eluent [22,25,27,28,34]. This is typically the case for high molecular weight solutes or for polymers in size exclusion chromatography. Several groups have nowadays provided clear experimental images of VF in chromatographic columns by magnetic resonance imaging [21–25] or direct optical visualization [29,30,33–38]. These visualizations allow to study both the onset of the instability as well as the later time nonlinear dynamics of the fingers. In order to improve quantitative analysis of these experimental data, several types of measurements inspired by the treatment of data in the physics literature can be performed. A first step in this direction has been given in [19,24,31,39–43] using dimensionless models of miscible VF. We have started to transpose the results in terms of dimensional quantities important in chromatographic applications focusing on the early onset time of the instability [19]. It is the goal of this article to complement this first study devoted to the linear stability analysis of miscible VF in packed chromatographic columns [19] by a similar treatment of the nonlinear dynamics occurring at later times. In particular, our study aims at showing the influence on the non-linear regime of various parameters such as the mean displacement velocity u, the longitudinal extension of the sample W, the column diameter d_c, the particle diameter d_p, the ratio between transverse and axial dispersion coefficient ϵ and the log–mobility ratio $R = \ln(\eta_2/\eta_1)$. We evaluate the influence of VF on the variance of the concentration distribution, a typical measure of the transport of viscous samples in chromatographic columns as viscous fingering leads to the deformation in time of the concentration peak either by broadening or by distortion. This can drastically affect the quality of the separation in various chromatographic circumstances. This is the case, for instance in preparative chromatography where highly concentrated – and thus highly viscous – sample solutions are used for increasing the productivity, or in size exclusion chromatography due to the large intrinsic viscosity of high molecular mass polymers, or still in two-dimensional liquid chromatography where fractions collected from a first column are displaced in a second one by another eluent of different viscosity.

The article is therefore organized as follows: in Section 2, we describe the physical model on which we base our numerical analysis and describe the numerical technique used to integrate the evolution equations. In Section 3, we review the typical phenomenology of non-linear VF and we focus on the numerical analysis of the influence of VF on the peak characteristics in chromatography before conclusions are drawn in Section 4.

2. Physical model and numerical implementation

We consider the displacement of two viscous and miscible fluids within a chromatographic column. A two-dimensional layer of viscous fluid 2 of width W (along the flow direction x) is confined between two regions of another less viscous fluid 1 (extending both upstream and downstream of the fluid 2 zone) in the porous medium the geometry of which is a rectangular domain of size $L_x \times L_y$. Fluid 2 represents the sample and fluid 1 the eluent. The sample is a solution of an unretained solute of initial concentration $c = c_2$ in the eluent. The solute concentration in fluid 1 is initially $c = 0$. Because mixing will modify the solute concentration c, the dynamic viscosity η of the sample will evolve as time goes according to the relationship $\eta = \eta(c)$. As usual, the velocity of the flow inside a porous medium with permeability k_p is governed by Darcy's law:

$$\mathbf{v} = -\frac{k_p}{\eta(c)}\nabla p \tag{1}$$

which relates the two-dimensional velocity $\mathbf{v} = (v_x, v_y)$ to the gradient of pressure p. v_x and v_y are the flow velocity components along the flow direction x and the transverse direction y, respectively. The flow is assumed to be incompressible ($\nabla \cdot \mathbf{v} = 0$). We have here assumed that the density of the two fluids is the same to simplify the problem and avoid further complexity related to possible buoyancy effects usually negligible in chromatographic applications [19]. The solute concentration evolves according to an advection-diffusion equation:

$$\frac{\partial c}{\partial t} + (\mathbf{v}\cdot\nabla)c = D_{ax}\frac{\partial^2 c}{\partial x^2} + D_{tr}\frac{\partial^2 c}{\partial y^2} \tag{2}$$

where D_{ax} and D_{tr} are the dispersion coefficients respectively along and transverse to the flow moving with the mean velocity u. This characteristic velocity is used to define a typical length scale $L_{ref} = D_{ax}/u$ and a typical time scale $\tau_{ref} = D_{ax}/u^2$ needed to nondimensionalize space and time. We nondimensionalize as well velocity components (both by u), the pressure (by $\eta_1 D_{ax}/k_p$ following Darcy's law), the concentration (by c_2) and the viscosity (by η_1, the viscosity of the eluent). From now on, a star superscript will denote a dimensionless quantity in the rest of the paper. As a consequence, the system is described by the following dimensionless equations:

$$\nabla^* . \mathbf{v}^* = 0, \tag{3}$$

$$\mathbf{v}^* = -\frac{1}{\eta^*(c^*)}\nabla^* p^* \tag{4}$$

and

$$\frac{\partial c^*}{\partial t^*} + (\mathbf{v}^*\cdot\nabla^*)c^* = \frac{\partial^2 c^*}{\partial x^{*2}} + \epsilon\frac{\partial^2 c^*}{\partial y^{*2}} \tag{5}$$

where we have introduced the ratio between the coefficients of dispersion $\epsilon = D_{tr}/D_{ax}$. Dispersion is isotropic (anisotropic) if $\epsilon = 1$ ($\epsilon \neq 1$). In order to get rid of the constant term due to advection at the mean flow velocity u and to better follow the fingering dynamics, we move to the Galilean frame of reference moving with constant speed u by defining $\tilde{x} = x - ut, \tilde{y} = y, \tilde{t} = t, \tilde{\mathbf{v}} = \mathbf{v} - u\mathbf{e}_x$ where $\mathbf{e}_x$ is the unit vector along the mean flow direction x. In dimensionless units, the Galilean transformations become

$$\tilde{x}^* = x^* - t^*, \tilde{y}^* = y^*, \tilde{t}^* = t^* \tag{6}$$

The dimensionless velocity is modified accordingly to

$$\tilde{\mathbf{v}}^* = \mathbf{v}^* - \mathbf{e}_x \tag{7}$$

We get the new system of equations in the moving frame:

$$\nabla^* \cdot \tilde{\mathbf{v}}^* = 0, \tag{8}$$

$$\tilde{\mathbf{v}}^* + \mathbf{e}_x = -\frac{1}{\eta^*(c^*)}\nabla^* p^* \tag{9}$$

and

$$\frac{\partial c^*}{\partial t^*} + (\tilde{\mathbf{v}}^*\cdot\nabla^*)c^* = \frac{\partial^2 c^*}{\partial \tilde{x}^{*2}} + \epsilon\frac{\partial^2 c^*}{\partial \tilde{y}^{*2}} \tag{10}$$

Both the pressure and concentration are invariant with respect to Galilean transformations. Moreover, we recall that, on the basis of Eqs. (6) and (7), we have that $\tilde{\nabla}^*() = \nabla^*()$ and $\partial()/\partial t^* = \partial()/\partial t^* + (\tilde{\mathbf{v}}^*\cdot\nabla^*)()$.

In order to close the system, we have to introduce the relationship between the evolving viscosity and concentration of the solute. Simulations on VF performed by the Physics community are frequently based on the assumption that the viscosity is an exponential function of the concentration, i.e. $\eta(c) = \exp(Rc)$ where R is the so-called log–mobility ratio defined as [1,8]:

$$R = \ln\left(\frac{\eta_2}{\eta_1}\right) \tag{11}$$

Although the viscosity of the chromatographic sample/mobile phase mixture is not always described by such a function, we keep it because, first, it is a simple law depending on a single parameter and, second, this corresponds to the empirical Arrhenius equation [45] which has sometimes been used to describe the viscosity behavior of chromatographic solvent mixtures [46,47]. If R is positive (as in our simulations), a low viscosity eluent 1 displaces a high viscosity sample 2 the rear interface of which is unstable with respect to VF. In the opposite case, it is the front interface of the sample which develops fingers. To solve the system of equations numerically, we eliminate the pressure gradient by taking the curl of Darcy's law in the moving frame and by introducing the so-called dimensionless stream function $\tilde{\psi}^*$ [10] whose space derivatives represent the velocity components:

$$\tilde{v}_{\tilde{x}}^* = \frac{\partial \tilde{\psi}^*}{\partial \tilde{y}^*} \quad \text{and} \quad \tilde{v}_{\tilde{y}}^* = -\frac{\partial \tilde{\psi}^*}{\partial \tilde{x}^*}. \tag{12}$$

We end up with a set of coupled equations for the stream function and the concentration:

$$\tilde{\nabla}^{*2} \tilde{\psi}^* = -R \left(\frac{\partial \tilde{\psi}^*}{\partial \tilde{x}^*} \frac{\partial c^*}{\partial \tilde{x}^*} + \frac{\partial \tilde{\psi}^*}{\partial \tilde{y}^*} \frac{\partial c^*}{\partial \tilde{y}^*} + \frac{\partial c^*}{\partial \tilde{y}^*} \right) \tag{13}$$

and

$$\frac{\partial c^*}{\partial \tilde{t}^*} + \frac{\partial \tilde{\psi}^*}{\partial \tilde{y}^*} \frac{\partial c^*}{\partial \tilde{x}^*} - \frac{\partial \tilde{\psi}^*}{\partial \tilde{x}^*} \frac{\partial c^*}{\partial \tilde{y}^*} = \frac{\partial^2 c^*}{\partial \tilde{x}^{*2}} + \epsilon \frac{\partial^2 c^*}{\partial \tilde{y}^{*2}}. \tag{14}$$

We use a pseudo-spectral code developed by Tan and Homsy [10] to integrate the model (13) and (14) on a two-dimensional domain of integration of size $L_y^* \times L_x^*$ where $L_y^* = L_y/L_{ref}$ is the dimensionless width of the porous medium (a control parameter) and $L_x^* = L_x/L_{ref}$ is the reduced axial length. In these conventions, L_x^* is related to the length of the column while L_y^* determines the number of fingers present across the domain. Indeed, as the fingering instability gives fingers with a characteristic wavelength λ, the averaged number of fingers observed at onset will be given by the ratio L_y^*/λ. The dimensionless length of the sample is $l = W/L_{ref}$. Initially, the rectangular sample with concentration $c^* = 1$ of size $L_y^* \times l$ is enclosed in the background motionless fluid where $c^* = 0$. For the purpose of visualization at various times of the VF pattern, which occurs on the upward side of the sample, the sample is shifted in the righter part of the integration domain and extends between $x_1^* = (4L_x^*/5 - l)$ and $x_2^* = 4L_x^*/5$.

In practice, for the simulations, the initial condition is the following:

$$c_0(x^*, y^*) = 0 \quad \text{for } 0 < x^* < x_1^* \tag{15}$$

$$c_0(x^*, y^*) = 0.5 + \xi r(y^*) \quad \text{at } x^* = x_1^* \tag{16}$$

$$c_0(x^*, y^*) = 1 \quad \text{for } x_1^* < x^* < x_2^* \tag{17}$$

$$c_0(x^*, y^*) = 0.5 + \xi r(y^*) \quad \text{at } x^* = x_2^* \tag{18}$$

$$c_0(x^*, y^*) = 0 \quad \text{for } x_2^* < x^* < L_x^* \tag{19}$$

where $\xi = 0.001$ is the amplitude of the random noise $r(y^*)$ while x_1^* and x_2^* are the initial positions of two back to back step functions between $c^* = 0$ and $c^* = 1$. There are thus two intermediate lines along y^* at $x_{1,2}^*$ where a random number r between 0 and 1 is added. This noise is necessary to trigger the fingering instability on reasonable computing time. If $\xi = 0$, the numerical noise will ultimately seed the fingering instability but on a much longer time scale (see [31] for a discussion on the influence of noise on the fingering pattern). Physically, the random numbers $r(y^*)$ relate to the microscopic noise inherent to any physical system while ξ relates to the degree of imperfections in the system. In a perfectly ordered and regular porous matrix, ξ would be very small and it would hence take time for the microscopic noise to be amplified.

In a macroscopically disordered system, imperfections correspond to a larger ξ susceptible to trigger VF more rapidly. As an example, Figs. 3 and 4 from the article by Fernandez et al. [22] compare VF measured experimentally in two columns, one with a quite heterogeneous packing (Fig. 3), the other one with a more regular packing (Fig. 4). VF appears much quicker in the first case which in our simulations would correspond to a larger ξ. However, as discussed in [31] (see Fig. 5 in this article), the amplitude ξ can slightly shift the onset time of the instability but no matter how small it is, VF will ultimately always appear.

The boundary conditions are periodic in both directions. This is quite standard for the transverse direction $\tilde{y}^*$. This does not make any problem along the $\tilde{x}^*$-axis as $c^* = 0$ at both $\tilde{x}^* = 0$ and $\tilde{x}^* = L_x^*$. The problem is controlled by four dimensionless parameters: the log–mobility ratio R, the dimensionless width of the column L_y^*, the initial length of the injected sample l and the ratio between transverse and longitudinal dispersion coefficients ϵ.

The numerical values of these four parameters are selected in such a way that they are representative of typical LC operating conditions. Thus, the column is assumed to be packed with particles of diameter d_p equal to 5 μm and to have an internal diameter d_c equal to 4.6 mm. The dimensional length W of the initial rectangular sample zone equals $d_c/4$, which, for a total porosity of 0.7, corresponds to an injection volume of 13.4 μl. The axial reduced plate height, $h_{ax} = H_{ax}/d_p$, where H_{ax} is the classical plate height describing dispersion along the column axis, is assumed to be related to the reduced velocity, ν, through the Knox semi-empirical equation [48]:

$$h_{ax} = \frac{B}{\nu} + A\nu^{1/3} + C\nu \tag{20}$$

where A, B and C are dimensionless constants. The reduced velocity ν is defined as [49]:

$$\nu = \frac{u d_p}{D_m} \tag{21}$$

where D_m is the solute molecular diffusion coefficient in the eluent, assumed equal to 0.5×10^{-5} cm^2 s^{-1}. The transverse reduced plate height, $h_{tr} = H_{tr}/d_p$, where H_{tr} is the transverse plate height defined as the rate of increase of the transverse variance of the concentration profile with axial distance migrated, is given by [50]:

$$h_{tr} = \frac{D}{\nu} + E. \tag{22}$$

The values of the dimensionless plate height coefficients are here selected equal to: $A = 1$, $B = 1.8$, $C = 0.01$, $D = 1.4$, $E = 0.06$. For comparison purposes, these typical values are the same as those selected and discussed in our previous publication on the linear stability analysis [19]. Because of the periodicity of the boundary conditions, the numerical code is most efficient when the dimensionless quantities L_y^* and L_x^* are multiples of prime numbers. Consequently, computations are performed by selecting ten values of L_y^* fulfilling this condition and for which the corresponding flow rate lies between 0.5 and 2.5 cm^3 min^{-1}. In practice, we take thus L_y^* from 512 to 820, i.e. explicitly 512, 528, 548, 576, 600, 628, 672, 720, 768, 820 hence l from 128 to 205. Therefore, since $L_y^* = d_c/L_{ref}$, the corresponding values of L_{ref} were calculated as d_c/L_y^*. Noting that $L_{ref} = D_{ax}/u = H_{ax}/2 = h_{ax}d_p/2$, the corresponding value of ν was obtained by solving Eq. (20) for ν, knowing that $h_{ax} = 2L_{ref}/d_p = 2d_c/(L_y^* d_p)$. The axial velocity u which does not appear explicitly as a control parameter in the model, influences nevertheless the results because it implicitly affects the reference length which is equal to half the axial plate height [19]. This axial velocity u is obtained from ν using Eq. (21) and ranges typically from 0.330 to 0.018 cm/s for L_y^* from 512 to 820. The knowledge of ν further allows to calculate h_{tr} from Eq. (22) from which the dispersion ratio ϵ equal to h_{tr}/h_{ax}

is computed. Although this parameter is rarely used in chromatography, it plays a significant role in the evolution of the VF pattern as will be seen in the next section. In practice, chromatographic columns are operated at quite low dispersion ratios. This ϵ ratio decreases with increasing v. For the above range of values of L_y^*, ϵ lies between 0.028 and 0.115.

3. Non-linear dynamics of viscous fingering and influence on output peaks

3.1. Linear vs. nonlinear approaches

Before describing the results of our numerical integration of model (13) and (14), it is useful to recall the difference between the information obtained from linear stability analysis as done in Ref. [19] and those gathered by studying the nonlinear dynamics as done here. When a hydrodynamic instability affects an interface such as in the here studied viscous fingering case, this results from the amplification by a destabilizing mechanism (the unfavorable viscosity ratio here) of small perturbations affecting the base state planar interface. These perturbations grow exponentially to conduct the system out of the unstable initial base state into the well developed unstable regime. As long as the perturbations δz of any variable z are small enough, all nonlinear terms of the evolution equations (for instance terms in δz^2) are negligible and the growth of the perturbations is well described by equations linearized in δz. This fixes the so-called "linear regime" in which perturbations are amplified exponentially. Analysis of this regime [19] provides information on the conditions to get instability and on the influence of the parameters on the onset time of the pattern and on its wavelength. Linear stability analysis cannot however give information on the long term evolution of the pattern dominated by the nonlinear interactions taking over when the perturbations become large enough for the nonlinearities of the equations to excite harmonics, etc. Nonlinear dynamics must then typically be studied by experiments or nonlinear simulations like done here.

3.2. Two-dimensional nonlinear dynamics

We display in Fig. 1 the nonlinear evolution in time of a finite band of a viscous sample pushed from left to right by a less viscous miscible displacing fluid also initially filling the chromatographic column. As we are interested in the long-time behavior in order to examine the effects of non-linearities, we do not display the relevant pictures associated with the linear growth of the instability which has been analyzed by linear stability analysis in [19]. The density plots of solute concentration are such that the maximum of dimensionless concentration c_{max}^* corresponds to black whereas $c^* = 0$ corresponds to white and intermediate values to grey levels. Of course, as the sample is diluted in the course of time both because of dispersion and fingering, the maximum value of concentration decreases (see also Fig. 2) so that the black zones at successive times in Fig. 1 correspond to decreasing values of c_{max}^*. Such a grey scale is used in order to amplify and track the fingers in the asymptotic regime. Note that Fig. 1 is shown in a frame moving with speed u. If u is increased, the view will thus be analogous however viscous fingering will be more intense as the system is more unstable when the injection speed is increased [8].

In Fig. 1, one clearly notices the appearance of several fingers which develop on the rear interface. At early times, fingers develop in both upstream and downstream directions around the unstable interface but as soon as the fingers traveling forward meet the frontal stable interface, reverse fingering is privileged [40]. Indeed, the frontal interface of the sample where the more viscous sample displaces the less viscous eluent is stable. It expands
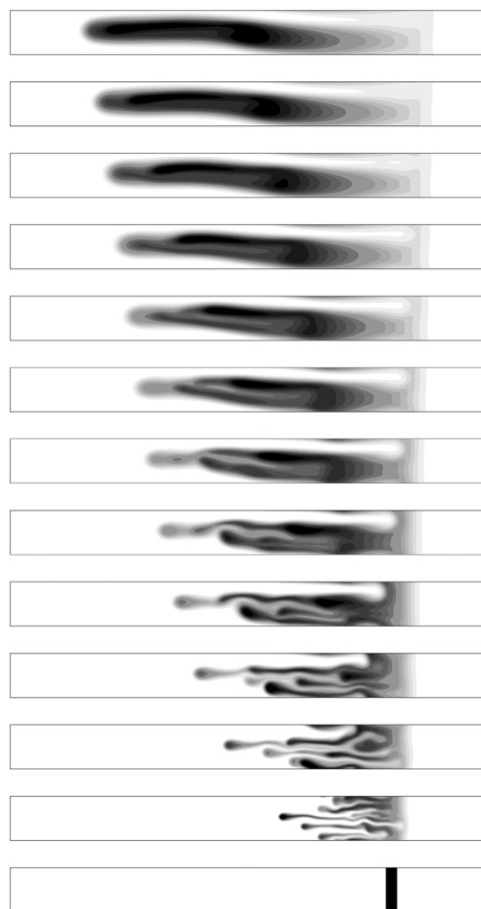

Fig. 1. Temporal evolution of nonlinear viscous fingering for a finite sample displaced from left to right by a less viscous flow. Density plots of concentration are shown at successive times from bottom to top in the frame moving at the injection speed u. Each picture is separated by 5000 units of dimensionless time, which corresponds to 31.9 s. Parameters are: $R = 2$, $L_y^* = 768$, $u = 0.094$ cm/s, $l = 192$, $\epsilon = 0.08722$. The aspect ratio is preserved.

only because of molecular diffusion and dispersion and remains planar until fingering of the rear interface is catching it. This stable barrier later on prevents the fingers from developing further downstream. Fig. 1 shows evidences of typical nonlinear events that have been described in details before [1,10,12,13]. First of all *fading* typically occurs when one finger is slightly ahead of a neighboring one. Because of the two flow vortices which accompany each finger head [44], the neighboring finger encounters an opposing flow created by the leading finger which hinders its growth. Hence, the neighboring finger is fading in time. This dynamics is favoring *merging* which occurs when one finger prefers to follow the slow resistance path set up by a neighboring finger rather than to act against the opposing flow created by it. Such fading and merging are clearly seen on panels 3–7 (from the bottom) from Fig. 1. Another nonlinear typical dynamics is *splitting* of fingers. This occurs when fingers have grown enough so that their tip is sufficiently large for the VF instability to operate again and split them into two. Such mechanisms are not encountered here in our simulations which use a too small lateral domain for this tip splitting to set in but have been experimentally [1,7] and numerically [10] described in details previously.

In Fig. 1, the combination of fading and merging leads eventually for the set of parameters used here to one single final finger. As a result, the frontal interface is now crossed by a stream of less viscous fluid. In this asymptotic dynamics, the growth of the mixing zone becomes dispersive again as has been discussed previously [31].
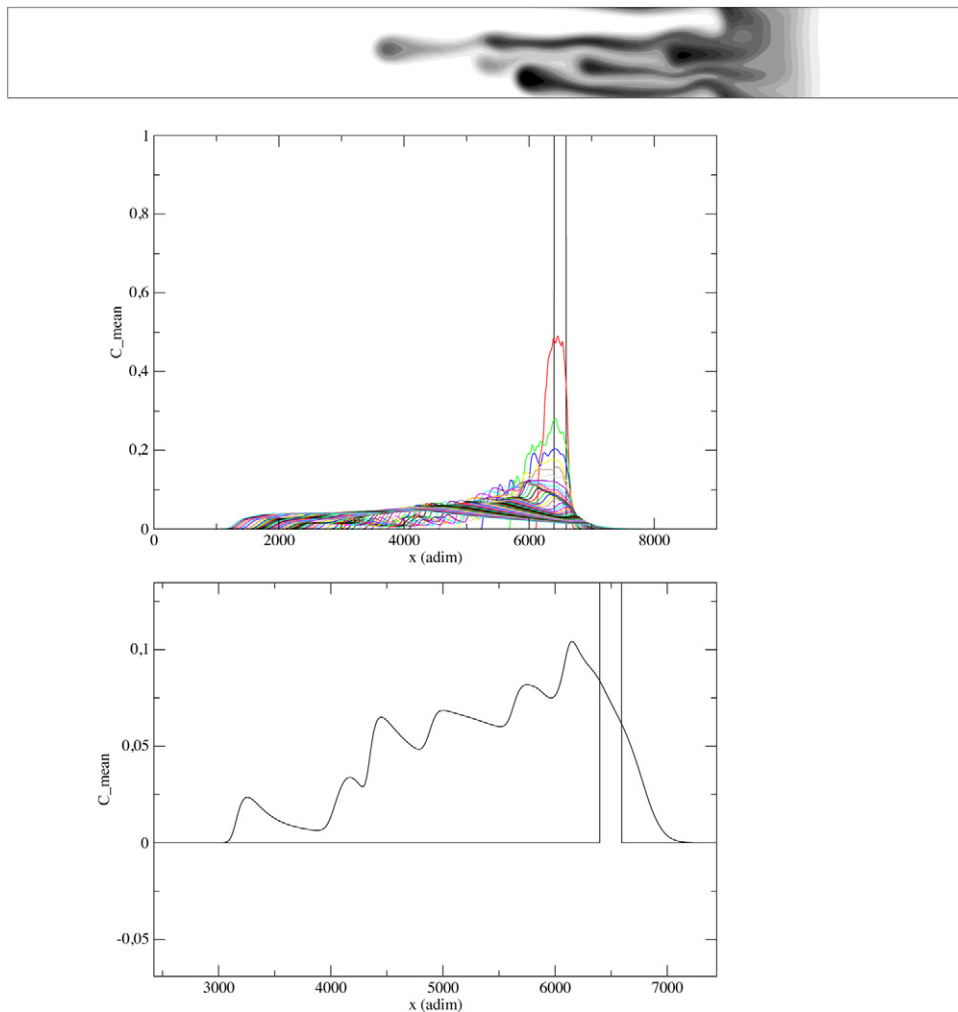
Fig. 2. Influence of viscous fingering on the peak broadening: (top) VF of Fig. 1 at $t^* = 15{,}000$; (middle) Corresponding transverse averaged profiles of the concentration as a function of space for different dimensionless times (up to 60,000); (bottom) transverse averaged profile at $t^* = 0$ and $t^* = 15{,}000$.

3.3. Influence of viscous fingering on characteristics of 1D output peaks

Is it possible to identify the appearance of viscous fingers only by looking at 1D averaged concentration profiles? This is crucial as, in all opaque columns, information on the internal dynamics have to be inferred from 1D profiles resulting from averages across the column width and measured by detectors at given positions along the column [11,17] or at the exit of it. We will now describe some quantities which can be related to those 1D averaged measures [51] and discuss how they correlate to the properties of nonlinear fingering.

As the 1D averaged profiles provide information on the integral of the concentration along the transverse cross-section of the column as a function of time, we first have to perform an averaging procedure of our numerical concentration field on the width of the sample. As a consequence, we plot in Fig. 2 the transverse averaged profile of the sample concentration at successive times t as a function of the longitudinal coordinate x in the frame of reference moving at the mean velocity u of the carrier fluid. This transverse averaged profile is defined according to the formula:

$$\bar{c}^*(\tilde{x}^*, t^*) = \frac{1}{L_y^*} \int_0^{L_y^*} c^*(\tilde{x}^*, y^*, t^*) dy^*. \tag{23}$$

One notices clearly in Fig. 2(b), which displays $\bar{c}^*(\tilde{x}^*, t^*)$ as a function of time, the stable forward front characterized by the

dispersion effect and the rear front which is unstable with regard to VF. The presence of fingers in the column is witnessed on the transverse averaged profile by the presence of bumps, a broadening of the concentration peak in time along with a shift of the center of mass of the sample in the direction reverse to the mean flow, indicating that this center of mass does not move along the column as fast as the carrier liquid.

A goal of this work is to investigate the long time contribution to the peak deformation due to the non-linear evolution of viscous fingering for a sample slice moving within a less viscous eluent. Hence, the asymptotic value of the variance associated to the concentration is fundamental in order to characterize the broadening of the initial slice [31,32,36,38]. Moreover, as the latter has a finite extension, it is of particular interest to study how fast axial dispersion in the chromatographic column is smoothing out the fingering instability. Indeed, if the transit time across the column is long, axial dispersion has a long time to dilute the sample in the x direction and thus to oppose to VF before the exit of the column.

To do so, we compute the two first moments of the concentration distribution: the dimensional first moment m (which has the dimension of a length), defined as

$$m(t) = \frac{\int_0^L \bar{c}(x, t) x \, dx}{\int_0^L \bar{c}(x, t) dx}, \tag{24}$$
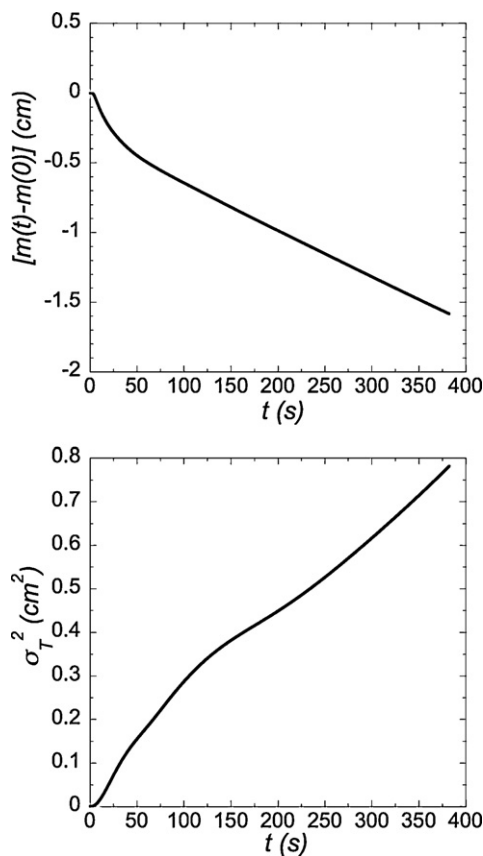
Fig. 3. Two first moments of the distribution in function of time for the simulation of Fig. 1: (top) mean position m of the center of mass; (bottom) variance.

is the position of the center of mass of the distribution as a function of time. In order to compare this position with that, m_0, that a zone unperturbed by VF would have, we subtract m_0 to it. Fig. 3(a) shows the evolution of the center of mass for the simulation of Fig. 1. The evolution is shown here in dimensional quantities in order to compare with the length of typical columns we consider (15 and 25 cm). To switch back from the dimensionless first moments computed on profiles of Fig. 2 using definition (24) to dimensional quantities, we use the characteristic time and length, t_{ref} and L_{ref}, computed as indicated at the end of Section 2. For the selected value of $L_y^* = 768$, this corresponds to a flow velocity of 0.094 cm/s, giving a reference length of 6.0 μm and a reference time of 6.4 ms.

In Fig. 3(a), the mean position of the center of mass is lower than that of a zone unperturbed by VF and their difference increases as a function of time. Hence, the distribution is going backward as the fingers are developing in the direction opposite to the mean flow. The advancing front somehow stabilizes the rear front since it avoids the fingers to grow in the flow direction. Hence, reverse fingering develops from the back interface.

The second dimensional moment of the $\overline{c}(x, t)$ distribution is the total variance σ_T^2

$$\sigma_T^2(t) = \frac{\int_0^L \overline{c}(x, t)[x - m(t)]^2 dx}{\int_0^L \overline{c}(x, t) dx} \tag{25}$$

giving information on the width of the distribution (in cm^2). Fig. 3(b) shows the temporal evolution of the dimensional total variance for the nonlinear simulation of Fig. 1. The total variance σ_T^2 is actually the sum of three contributions:

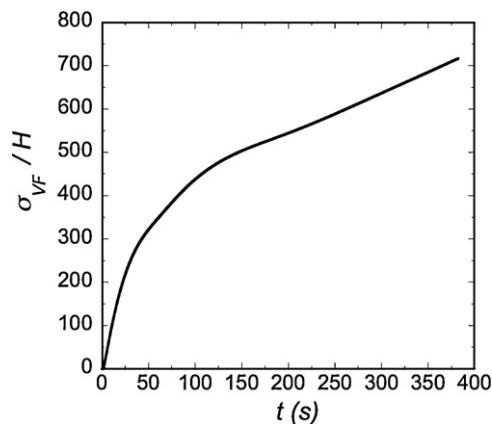$$\sigma_T^2(t) = \sigma_i^2 + \sigma_d^2 + \sigma_{VF}^2, \tag{26}$$

Fig. 4. Number of plates occupied by the viscous fingering contribution to the zone standard deviation along the chromatographic column as a function of time.

where $\sigma_i^2 = W^2/12$ is the variance due to the initial width of the sample, $\sigma_d^2 = 2D_{ax}t$ is the contribution of dispersion and σ_{VF}^2 is the contribution due to the fingering phenomenon. To understand the importance of VF on the broadening of the peaks, we isolate the temporal evolution of σ_{VF} defined as

$$\sigma_{VF} = \sqrt{\sigma_T^2 - \sigma_i^2 - \sigma_d^2}. \tag{27}$$

In order to better visualize the importance of the VF contribution to peak broadening, this axial contribution σ_{VF} is plotted in Fig. 4 vs. time in terms of the axial plate height, H_{ax}. Hence, the ordinate of Fig. 4 represents the number of plates occupied by this VF standard deviation. It increases quickly at early times, then less quickly as time goes by, until it eventually reaches a plateau value for longer times (exceeding 400 s).

3.4. Statistically averaged quantities

It is now clear that measurements of the moments of 1D averaged concentrations distributions can be related to the properties of VF. It is however important to realize that any such quantitative measures will have to imply statistical averages on several experiments performed in the same conditions. Indeed, as already evidenced numerically in the past [31] and shown recently experimentally [35], even if the fingering pattern is quite reproducible at onset, the nonlinear evolution and interaction of fingers greatly depends on the noise in the system. At onset, the wavelength of the pattern is the one of the most unstable mode given by the linear stability analysis [19]. At later times, the nonlinearities of the evolution equations excite the harmonics of this mode and of all other unstable modes so that a whole band of unstable modes start to interact. The corresponding dynamics is of course very sensitive to the initial noise.

In order to demonstrate the influence of noise realization on the temporal evolution of viscous fingering, we show in Fig. 5 density plots of concentration for exactly the same parameters as in Fig. 1. Each condition is the same, the only difference is in the realization of random numbers $r(y^*)$ used to seed the initial condition (15)–(19) in the simulation. In other words, the *amplitude* ξ of the noise is identical but it is only the values of the random numbers in the *realization* $r(y^*)$ which is different. We clearly observe in Fig. 5 that, at the same final time of 60,000, we have now two fingers instead of the final single finger of Fig. 1. In addition, we remark here the creation and the detachment of a drop of more viscous fluid in the rear at 10, 000 units of times, a feature absent in Fig. 1. Hence, noise has a drastic influence on the initiation and evolution of the instability associated to viscous fingering. This

Fig. 5. Same as Fig. 1. All values of parameters are the same, the only difference is a different initial noise with identical amplitude ξ but a different set of random numbers $r(y^*)$ in the initial condition (15)–(19).

Fig. 6. Standard deviation rescaled by the column length as a function of the dimensional mean velocity u. The "error bars" correspond to the range of variances obtained for different noise realizations with identical amplitude. The parameters are obtained as described in the text. The dots and squares correspond to a column with total length 15 cm and 25 cm respectively.

random generation of noise which initiates the development of the VF instability reflects the various uncontrolled sources, internal or external to the column itself, which, in practice, trigger this instability. As a consequence, the temporal evolution of the variance will depend on the specific realization of the experiment. Any quantitative information on parametric dependence of the influence of VF on this variance will therefore require the computations of an averaged variance obtained by averaging on different realizations for the same operating conditions.

3.5. Parametric study

To do so, we have performed for each set of values of the simulation parameters (R, L_y^*, l, ϵ), 15 different simulations starting from an initial condition where the amplitude ξ of the noise is the same but the realization r is each time different. From there we compute the average value $\langle \sigma_{VF} \rangle$ [31] which we will now analyze comparing two chromatographic columns with different typical lengths L_c (15 and 25 cm).

For each realization of a given set of the simulations parameters, the variance of the spatial distribution of the concentration is computed at the dimensionless time t^* corresponding to the hold-up time, L_c/u, i.e. at $t^* = 2L_c/H_{ax} = 2N$, where N is the column plate number in absence of VF. The VF contribution σ_{VF} to the standard deviation of the elution peak is then extracted from this variance by means of Eq. (27). In Fig. 6, the average, $\langle \sigma_{VF} \rangle$, of the resulting standard deviations obtained for the fifteen realizations of a given set of simulation parameters at the elution time is rescaled by the
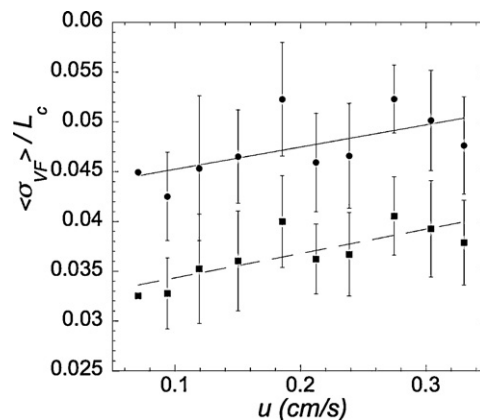
column length L_c and plotted as a function of the flow velocity. The upper and lower data correspond to column lengths of 15 cm and 25 cm, respectively. It should be noted that the rescaling of the VF standard deviation by L_c is just performed to express it in an easily visualized way, not to imply that it would correspond to some universal normalization.

It is seen that the VF contribution to the peak standard deviation increases only slightly with increasing flow rate. This might appear to be reminiscent of the fact that the maximum growth rate of the VF instability was found to increase with increasing flow velocity in its linear regime [19]. However, such a conclusion is not trivial, first because the development of the fingers in the column occurs mostly in the nonlinear regime, and second, because the larger the flow velocity, the shorter the time allowed to the VF instability to develop before reaching the column outlet. Nevertheless, the extent of this VF contribution to the peak standard deviation is quite significant and reaches about 4.5% and 3.5% of the length for the short (15 cm) and long (25 cm) columns, respectively. For the sake of comparison, the injection contribution σ_i to the standard deviation is respectively 0.22% and 0.13%, while that of the normal dispersion process σ_d ranges between 0.83% and 1.09% in the velocity interval covered in Fig. 6 for the short column and between 0.64% and 0.85% for the long column. The error bars reported in Fig. 6 correspond to the standard deviation of the variations of σ_{VF} for the various realizations. Its relative value lies between 10% and 15%.

Furthermore, whatever the flow velocity, the VF contribution to the peak standard deviation relative to the column length is observed to be larger for the short column than for the long one. This indicates that, whatever the selected flow velocity, the VF standard deviation grows less rapidly than the column length (and hence than the elapsed time), as reflected by Fig. 4.

One of the key parameters controlling the development of the VF instability is the ratio between transverse and axial dispersion coefficients, ϵ, i.e. the ratio of the transverse and axial plate heights. This parameter is usually not determined in chromatography as it does not significantly affect the separation performance. However, compared to other situations involving flow in a porous medium, a peculiarity of modern liquid chromatography is that this ratio is quite small. As this ratio is a monotonic decreasing function of the reduced velocity, the data $\langle \sigma_{VF} \rangle / L_c$ of Fig. 6 are plotted vs. ϵ in Fig. 7. The average VF contribution to the peak standard deviation is seen to be a decreasing quasi-linear function of ϵ. On a physical ground, this reflects the fact that the development of the VF instability is dampened when transverse mixing is enhanced,

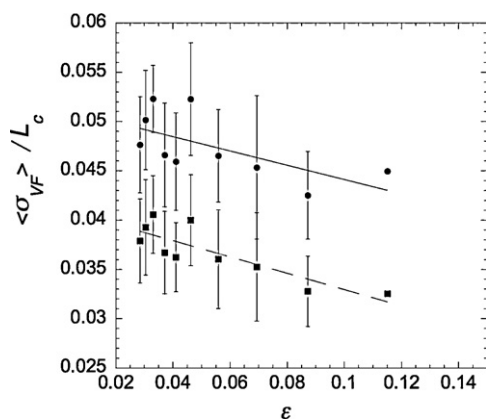**Fig. 7.** Standard deviation rescaled by the column length as a function of the ratio between transverse and axial dispersion coefficients ϵ. Symbols are the same as in Fig. 6.

compared to longitudinal mixing, resulting in an enhanced merging of neighbor fingers.

4. Conclusion

We have here summarized the various properties of nonlinear fingering of finite width samples in the context of chromatographic applications and shown numerically how useful quantitative data can be extracted from experiments. We have in particular shown that a useful measure is $\langle \sigma_{VF}(t) \rangle$, the ensemble average contribution of VF to the standard deviation of the transverse averaged concentration profiles. Typically this quantity gives the contribution of VF on peak broadening in time. We have shown that this broadening is a slightly increasing function of the flow velocity but a decreasing function of ϵ, the ratio between transverse and axial dispersion coefficients.

One could argue that the quantities measured here will be of no use in the case of chromatographic data such as those shown in [21–25,29,30,33–35,37] because their pictures are 2D visualizations of a full 3D dynamics. Zimmerman and Homsy have compared transverse averaged quantities of respectively 2D and full 3D simulations of VF showing that the averaged quantities remain the same [13]. In that regard, a welcome experimental work would be to compare statistical moments of the 1D transverse averaged profiles as defined in this work of a full 3D experimental dynamics in a column to those of 2D pictures of it in the same experiment. This would allow to check whether the equivalence of averaged properties of 2D vs. 3D numerical data remains valid for experimental ones.

Our analysis has furthermore emphasized the switch from dimensionless quantities such as those obtained from nonlinear simulations to dimensional quantities to be compared to experiments. The key experimental parameters that are required for this purpose are the geometrical dimensions of the column (length and internal diameter), the dispersion ratio or ratio of transverse to axial plate height (which itself depends on the flow velocity, particle diameter, molecular diffusion coefficient and coefficients of transverse and axial plate height curves) and the sample-to-mobile phase viscosity ratio (rather than their viscosity difference). The switch to dimensional quantities has proven to be of peculiar interest to understand the influence of the injection speed u on VF. As this mean displacement velocity is implicitly hidden within the characteristic length L_{ref} and time τ_{ref} needed to nondimensionalize the problem, it is hard to appreciate its influence on the spreading of peaks in dimensionless units. Switching back to dimensional units has allowed here to show explicitly (see Fig. 6) that the VF

contribution to the increase of the standard deviation of the output peaks varies only slightly with the injection speed u.

The present simulations have been performed under the assumption that the viscosity of the sample and mobile phase mixture is a monotonic function of the composition, characterized by a constant value of R. Work is in progress for handling mixtures which exhibit an extremum in their viscosity vs. composition curves leading to non-monotonic viscosity profiles [52]. The goal is to approach the situation of methanol–water or acetonitrile–water mixtures frequently encountered in reverse phase liquid chromatography and in hydrophilic interaction liquid chromatography (HILIC). Furthermore, the present simulations correspond to isocratic elution conditions. The influence of viscous fingering in gradient elution conditions will be the topic of a future publication. Note that the medium has here also been considered as homogeneous. Analysis of the influence of heterogeneities [53] could as well be the topics of future studies.

References

[1] G.M. Homsy, Annu. Rev. Fluid Mech. 19 (1987) 271.
[2] J. Nittmann, H.E. Stanley, Nature 321 (1986) 663.
[3] K.V. McCloud, J.V. Maher, Physics Reports 260 (1995) 139.
[4] P.G. Saffman, G. Taylor, Proc. R. Soc. London Ser. A 245 (1958) 312.
[5] R.A. Wooding, J. Fluid Mech. 39 (1969) 477.
[6] H.S. Hele-Shaw, Trans. Inst. Naval Architects London 40 (1898) 21.
[7] R. Maes, G. Rousseaux, B. Scheid, M. Mishra, P. Colinet, A. De Wit, Phys. Fluids 22 (2010) 123104.
[8] C.T. Tan, G.M. Homsy, Phys. Fluids 29 (1986) 3549.
[9] Y.C. Yortsos, Phys. Fluids 30 (1987) 2928.
[10] C.T. Tan, G.M. Homsy, Phys. Fluids 31 (1988) 1330.
[11] J.-C. Bacri, D. Salin, R. Wouméni, Phys. Rev. Lett. 67 (1991) 2005.
[12] W.B. Zimmerman, G.M. Homsy, Phys. Fluids A 3 (1991) 1859.
[13] W.B. Zimmerman, G.M. Homsy, Phys. Fluids A 4 (1992) 1901.
[14] A. Rogerson, E. Meiburg, Phys. Fluids A 5 (1993) 2644.
[15] O. Manickam, G.M. Homsy, Phys. Fluids A 6 (1994) 95.
[16] P. Petitjeans, C.Y. Chen, E. Meiburg, T. Maxworthy, Phys. Fluids 11 (1999) 1705.
[17] V. Kretz, P. Berest, J.-P. Hulin, D. Salin, Water Res. 39 (2003) 1032.
[18] M.N. Islam, J. Azaiez, Int. J. Numer. Methods Fluids 47 (2005) 161.
[19] G. Rousseaux, A. De Wit, M. Martin, J. Chromatogr. A 1149 (2007) 254.
[20] M. Czok, A. Katti, G. Guiochon, J. Chromatogr. 550 (1991) 705.
[21] L.D. Plante, P.M. Romano, E.J. Fernandez, Chem. Eng. Sci. 49 (1994) 229.
[22] E.J. Fernandez, C.A. Grotegut, G.W. Braun, K.J. Kirschner, J.R. Staudaher, M.L. Dickson, V.L. Fernandez, Phys. Fluids 7 (1995) 468.
[23] E.J. Fernandez, T.T. Norton, W.C. Jung, J.G. Tsavalas, Biotechnol. Prog. 12 (1996) 480.
[24] T.T. Norton, E. Fernandez, Ind. Eng. Chem. Res. 35 (1996) 2460.
[25] M.L. Dickson, T.T. Norton, E.J. Fernandez, AIChE J. 43 (1997) 409.
[26] D. Cherrak, E. Guernet, P. Cardot, C. Herrenknecht, M. Czok, Chromatographia 46 (1997) 647.
[27] R.C. Castells, C.B. Castells, M.A. Castillo, J. Chrom. A 775 (1997) 73.
[28] C.B. Castells, R.C. Castells, J. Chromatogr. A 805 (1998) 55.
[29] B.S. Broyles, R.A. Shalliker, D.E. Cherrak, G. Guiochon, J. Chromatogr. A 822 (1998) 173.
[30] R.A. Shalliker, B.S. Broyles, G. Guiochon, J. Chromatogr. A 865 (1999) 73.
[31] A. De Wit, Y. Bertho, M. Martin, Phys. Fluids 17 (2005) 054114.
[32] S. Keunchkarian, M. Reta, L. Romero, C. Castells, J. Chromatogr. A 1119 (2006) 20.
[33] H.J. Catchpoole, R.A. Shalliker, G.R. Dennis, G. Guiochon, J. Chromatogr. A 1117 (2006) 137.
[34] R.A. Shalliker, H.J. Catchpoole, G.R. Dennis, G. Guiochon, J. Chromatogr. A 1142 (2007) 48.
[35] R.A. Shalliker, V. Wong, G. Guiochon, J. Chromatogr. A 1161 (2007) 121.
[36] R.A. Shalliker, G. Guiochon, J. Chromatogr. A 1216 (2009) 787.
[37] R.A. Shalliker, G. Guiochon, Analyst 135 (2010) 222.
[38] W. De Malsche, J. Op De Beeck, H. Gardeniers, G. Desmet, J. Chromatogr. A 1216 (2009) 5511.
[39] M. Mishra, M. Martin, A. De Wit, Phys. Fluids 19 (2007) 073101.

[40] M. Mishra, M. Martin, A. De Wit, Chem. Eng. Sci. 65 (2010) 2392.
[41] C.-Y. Chen, S.-W. Wang, Int. J. Num. Meth. Heat Fluid Flow 11 (2001) 761.
[42] M. Mishra, M. Martin, A. De Wit, Phys. Rev. E 78 (2008) 066306.
[43] M. Mishra, M. Martin, A. De Wit, Phys. Fluids 21 (2009) 083101.
[44] A. De Wit, G.M. Homsy, J. Chem. Phys. 110 (1999) 8663.
[45] S. Arrhenius, Z. Phys. Chem. 1 (1887) 285.
[46] M. Martin, G. Guiochon, J. Chromatogr. 151 (1978) 267.
[47] L.R. Snyder, J.J. Kirkland, Introduction to Modern Liquid Chromatography, 2nd ed., Wiley, New York, 1979, pp. 836–839.
[48] J.N. Done, G.J. Kennedy, J.H. Knox, in: S.G. Perry (Ed.), Gas Chromatography 1972, Applied Science Publ., Barking, UK, 1973, p. 145.
[49] J.C. Giddings, Nature 184 (1959) 357.
[50] J.H. Knox, G.R. Laird, P.A. Raven, J. Chromatogr. 122 (1976) 129.
[51] M.P.M.A. Baroni, A. De Wit, R.R. Rosa, Europhys. Lett. 92 (2010) 64002.
[52] O. Manickam, G.M. Homsy, Phys. Fluids 6 (1994) 95.
[53] A. De Wit, G.M. Homsy, J. Chem. Phys. 107 (1997) 9619.